Numerical simulation of fire whirls

Rui Miguel Godinho Parente
rui.parente@tecnico.ulisboa.pt

Instituto Superior Técnico, Universidade de Lisboa, Portugal

November 2018

Abstract

This work presents a numerical study of laboratory fire whirls. The Reynolds Stress Transport turbulence model RST is used together with Eddy Break-Up combustion and radiation models. The unsteady 3D fire whirl prediction assume the same swirl generator used in the laboratory consisting on enclosure walls to constrict airflow to enter tangentially in the facility. A low momentum fuel jet is located at the bottom centre of two halves of an offset hollow cylinder. A detailed comparison between available experimental data and numerical predictions, ranging from 2 to 300 kW is presented. The results are in good agreement with the available experimental data and confirm that the Burgers vortex gives a good description of the flow kinematics. The flame height dependence on circulation was deduced using scaling laws and validated with experimental data. For each heat release considered, a critical circulation was found that results in a maximum flame height. Turbulence fields predictions are discussed in light of the role of turbulent suppression and Richardson parameters.
Keywords: Fire whirls, CFD, RST, Flame Height, Circulation, Scaling analysis

Nomenclature

β_λ	Extinction coefficient
$\dot{m}_0$	Fuel mass flow at the burner [Kg/s]
$\kappa_{a\lambda}$	Absorption coefficient at wavelenght λ
$\kappa_{pa\lambda}$	Particle absorption coefficient at wavelength λ
$\kappa_{s\lambda}$	Scattering coefficient at wavelength λ
Ω	Solid angle
D	Facility diameter [m]
D_0	Burner diameter [m]
H	Facility height [m]
H_f	Flame height [m]
$I_{b\lambda}$	Black body intensity at wavelength λ
r_v	Vortex radius [m]
S	Slit gap width [m]
V_m	Maximum tangential velocity [m/s]

1. Introduction

Fire whirls are dangerous flame structures that arise from the interaction of buoyant flames and ambient vorticity. They may appear on forest and urban fires. This phenomenon is associated with strong swirling buoyant fire motion, originating an increase in burning rates compared with normal fires. The vertical momentum is strong enough to lift and toss burning debris over large distances, making difficult the fire extinction. In addition, their unexpected occurrence behaviour and large radiative heat fluxes, represent great danger specially for firefighters and also for inhabitants, as remembered on the historical Tokyo disaster, where 38000 people were killed [1] and the Chicago fire in 1871 responsible for 300 fatalities [2].

Fire whirls are originated on the ground as reviewed recently by [3] and require three major mechanisms

i) a heat source responsible for create a buoyancy force, ii) a vorticity generation mechanism in order to create a rotational field and iii) surface drag force to create a radial boundary layer that facilitates the air entrainment into the vortex and increases the vorticity generation.

The experimental study of fire whirls is usually carried on adopting two kind of heat sources, a fixed heat release such as low momentum burners [4, 5] or solid fuels [6] and pool burning [7, 8]. The fire whirl geometrical configurations are designed to promote the required entrainment with tangential momentum.

Usually they consist of an enclosure facility with rotating side walls or fixed walls with slits to promote tangential entrainment. A few others mechanisms are used such as obstacles that generate vortical structures [9, 10] or fire merging and multiple flames [11, 12, 13]. The different types of enclosure facilities have been reviewed by Tohidi *et al.* [3].

The complexity associated with the fire whirl phenomenon is well illustrated with the existence of 13 non dimensional groups [3] that govern the phenomenon. Unfortunately, the number of permutations required to investigate the influence of 13 non dimensional groups is prohibitive. Nevertheless, some authors have focussed their description on a few non dimensional parameters relating flame height as a function of circulation and mass flow consumption as a function of circulation [4, 7, 9, 10, 14].

The dramatic increase of flame height observed in fire whirls compared with analogue non swirling flames is presented not only on pool fire where the fuel consumption increases, but also on burners with constant rate of fuel supply.

The influence of the entrainment gap width on the flame height and stability of fire whirls was investigated by Yu *et al.* [15] using a fixed frame facility, which concluded that for small gap widths no fire whirl was observed. Battaglia *et al.* [16] and Zhou and Wu [13] reported that low circulation values have a negative impact on the flame height. Hartl and Smits [4] and Forthofer and Goodrick [2] reported that flame height increases with circulation. Snegirev *et al.* [17] observed that the flame height increase with circulation, reaching the highest value when the swirl number was equal to 0.6. Lei *et al.* [18] concluded that the circulation for which the flame height is maximum depends on the heat release. Further increase in circulation will result in a decrease on the flame height. Finally, for extreme high circulation vortex breakdown may occur decreasing the flame height, see e.g Tohidi *et al.* [3] Zhou *et al.* [19] and Lei *et al.* [18]. Despite of the effort of studying fire whirls, the fundamental knowledge of the driving mechanism and physical behaviour is still not fully understood.

The complexity of the phenomenon also create modelling difficulties and very few numerical studies have been validated against experimental data. Battaglia *et al.* [16] reported one of the first attempts in numerical modelling of fire whirls simulation using FDS computer code with Large Eddy Simulation in order to recreate the pioneer experimental work of Emmons and Ying [20]. Others FDS simulation studies have followed like Yuen *et al.* [21] which recreated the experimental work of Chow *et al.* [22] but the temperature field was over predicted while Zou *et al.* [23] reported reasonable agreement with the measured flame height and centre line temperature profiles.

The few reported simulations do not include validation of the turbulent field of the fire whirl. It is well know the lack of performance of two equation turbulence models as $\kappa - \epsilon$ to simulate flows dominated by buoyancy and swirl, see e.g. Hanjalic [24] and Pereira and Rocha [25, 26]. Several models extension of the standard $\kappa - \epsilon$ have been proposed. Chow *et al.* [22] used the RNG $\kappa - \epsilon$ from the commercial code FLUENT to validate the assumption of a Burgers vortex flow behaviour on the fire whirl core, but only the flame height was compared with the experimental work. Other two equation turbulence models variants were compared, see e.g Snegirev *et al.* [17], but second order closures offer better prospects than eddy viscosity models for capturing at least some of the complex phenomenon of buoyant turbulent flows. Consequently numerical simulation of fire whirls constitute a great challenge due to the modelling but also the computational power required if LES modelling is selected.

The first objective of this work is to validate the 3D unsteady simulations against several fire whirl experiments ranging from 2 to 300 kW. The second objective is to investigate numerically the role of circulation on the flame height and flame structure. Finally, the role of turbulence suppression on the flame height elongation of turbulent fire whirls is investigated.

Next section describes the mathematical and numerical models as well as the geometrical configurations. The third section deals with the validation issue for the velocity, temperature and flame height compared with reported data from different fire whirls. This is followed in section four by the discussion of the circulation, power and turbulence on the fire whirl flame height. The paper finishes with summary conclusions.

2. Numerical Modelling

2.1. Governing Equations

The time averaged form of the compressible Navier-Stokes equations for the continuity, momentum and

energy equation read as:

$$\frac{\partial \rho}{\partial t} + \nabla \cdot \left[\rho \bar{V}\right] = 0 \tag{1}$$

$$\frac{\partial}{\partial t}\left(\rho \bar{V}\right) + \nabla \cdot \left[\rho \bar{V}\bar{V}\right] = -\nabla \cdot pI + \nabla \cdot (T + T_t) + f_b$$

$$\frac{\partial}{\partial t}\left(\rho E\right) - \nabla \cdot \left(V\left(\rho E - P\right)\right) = \nabla \cdot \left[\left(K + \frac{C_p \mu_t}{Pr_t}\right)\nabla \cdot T + V(T_f)\right] + S_h$$

where I is the identity tensor, T is the viscous stress tensor, T_t the Reynolds stress tensor, T_f the turbulent heat flux vector and f_b is the resultant of the body forces (such as gravity).

2.2. Physical modelling

i)Turbulence Model

The time average Navier-Stokes and energy equations were close by RST, where all components of the Reynolds Stress Tensor are directly computed by a transport equation. In the RST model the transport equation for the specific Reynolds stress tensor $R = \frac{-T_f}{\rho}$ is defined as follows:

$$\frac{\partial}{\partial t}\left(\rho R\right) + \nabla \cdot \left(\rho R \bar{V}\right) = \nabla \cdot D + P + G - \frac{2}{3}\rho I \gamma_M + \underline{\phi} + \underline{\epsilon} + S_r \tag{2}$$

where γ_M is the Dilatation Dissipation, $\underline{\epsilon}$ is the turbulent dissipation rate tensor and S_R is a specified source. The generalized gradient diffusion (D) was used for the turbulent heat flux vector.

ii)Combustion Model

The Eddy Break Up (EBU) model from Spalding [27] and Magnussen and Hjertager [28] was selected. The individual species are transported at different rates according to their own governing equations. The time average of the instantaneous governing equations can be written as follows:

$$\frac{\partial}{\partial t}\left(\rho \chi \bar{Y}_i\right) + \nabla \cdot \left(\rho U \bar{Y}_i - \bar{F}_i\right) = \bar{S}_i \tag{3}$$

where F_i is the diffusion flux and is defined as:

$$F_i = \left(D_i + \frac{\mu_t}{Sc_i}\right)\nabla \bar{Y}_i \tag{4}$$

The mixing controlled rate of reaction is expressed in terms of the turbulence time scale $\frac{\kappa}{\epsilon}$. The individual dissipation rates for fuel, oxygen and combustion products are expressed as follows:

$$\dot{w}_{fu} = C_r \bar{\rho} Y_{fu} \frac{\epsilon}{\kappa} \tag{5}$$

$$\dot{w}_{ox} = C_r \bar{\rho} \frac{Y_{ox}}{s} \frac{\epsilon}{\kappa} \tag{6}$$

$$\dot{w}_{pr} = C_r \bar{\rho} \frac{Y_{pr}}{1+s} \frac{\epsilon}{\kappa} \tag{7}$$

For the actual reaction rate of fuel, the EBU takes into account the individual dissipation rates, eqs. (5) to (7), and assumes that it is equal to the slowest one:

$$R_f = -\rho \frac{\epsilon}{\kappa} min\left[C_r Y_{fu}, C_r \frac{Y_{ox}}{s}, C_r \frac{Y_{pr}}{1+s}\right] \tag{8}$$

iii)Radiation

As radiation travels through a participating media the material that is present in the media, can absorb, emit or scatter radiation. The effect on the radiant intensity is governed by the following equation:

$$\frac{\partial I_\lambda}{\partial s} = -\beta_\lambda I_\lambda + \kappa_{a\lambda} I_{b\lambda} + \frac{\kappa_{s\lambda}}{4\pi}\int_{4\pi} I_\lambda(\Omega)\partial(\Omega) + \kappa_{pa\lambda} I_{pb\lambda} + \frac{\kappa_{ps\lambda}}{4\pi}\int_{4\pi} I_\lambda(\Omega)\partial(\Omega) \tag{9}$$

The field equation for radiation intensity is solved with the Discrete Ordinates Method (DOM):

$$s_i \cdot \nabla I_{i\delta\lambda} = -\beta_{\delta\lambda} I_{i\delta\lambda} + \kappa_{a\delta\lambda} I_{b_\delta\lambda} + \frac{\kappa_{s\delta\lambda}}{4\pi}\sum_{j=1}^{n} w_j I_{j\delta\lambda} + \kappa_{\bar{p}\delta\lambda} I_{p\delta\lambda} + \frac{\kappa_{\bar{p}\delta\lambda}}{4\pi}\sum_{j=1}^{n} w_j I_{j\delta\lambda} \tag{10}$$

Finally, the absorption coefficient is calculated with the Weighted Sum of Gray Gases (WSGG). This method makes use of the Hottel charts and sum-of-gray-gases models for a mixture containing CO_2 and/or H_2O gases only. The total absorptivity is computed as follow:

$$a \approx \sum_{\kappa=0}^{\kappa} a_\kappa \left(1 - e^{-K_\kappa S}\right) \tag{11}$$

where K is the total number of gray gases, a_κ is the weight factor, K_κ is the absorption coefficient of each gray gas and S is the optical thickness.

2.3. Geometry configuration and boundary conditions

Figure 1 shows the fire whirl generator geometry comprising two half staggered cylinders located at

the centre of the computational domain. The facility dimensions are listed on table 1. The origin of the Cartesian coordinate system is centred at the base of the burner.
The burner is modelled as a mass flow inlet with the fuel mass fraction set to one. Due to the large gradients on the base of the fire whirl, the burner boundary condition was extended downward. Additionally, in order to avoid back fire, for $z < 0$ a porous medium was modelled with (pressure drop) source terms on the momentum equation. The far field

Heat Release (kW)	D_0(m)	D(m)	S(m)	H(m)
2	0.0381	0.305	0.0762	0.890
5	0.0381	0.305	0.0381	0.890
50	0.3	2	0.4	15
150	0.3	2	0.4	15
300	0.3	2	0.4	15

Table 1: Geometry details for simulated cases

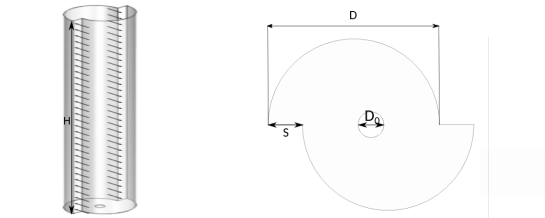

(a) Geometry used (b) Top View

Figure 1: Fire whirl generator

boundary were modelled as pressure outlet with prescribed pressure ($p_{working} = p_{static} - \rho_{ref} \cdot g \cdot \partial h$) set to zero relative to the atmospheric pressure. The no slip boundary velocity condition was assigned to all physical walls.
The computational domain was discretized with 1.8 million trimmed cells. The mesh comprises four different blocks with refinement, see figure 2. Prism layers were used on the bottom boundary for better discretization of the high gradients on the formation of fire whirls and vorticity generation. The

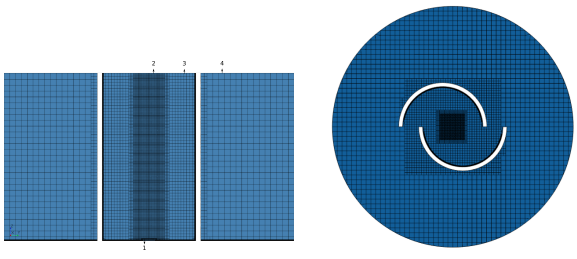

(a) Front view (b) Top View

Figure 2: Example of the mesh generated.

software Star-CCM+ ® (version 12.04) was used and employs second order numerical accuracy on unstructured meshes and is widely used by the authors, see e.g [29].

3. Results

The numerical simulation were validated with experimental data obtained in fire whirls by Hartl and Smits [4] and Lei *et al.* [30]. They were obtained for different inlet burner powers raging from 2 to 300 kW.
Figure 3a) shows the predicted mixture fraction stoichiometric isosurface for 300 kW around the cylindrical fire whirl, with 15 burner diameters in height, together with the spiral streamlines configuration. Figure 3b) shows a tangential velocity profile on the radial direction compared with an analogous profile from the analytical solution of a Burgers vortex. The obtained good agreement suggests that the Burgers vortex describes well the flow kinematics in agreement with other authors [4, 30, 31, 32].

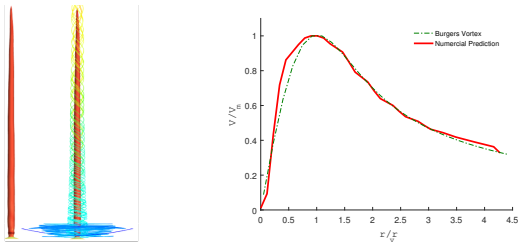

(a) Stoichiometric mixture fraction isosurface (b) Tangential velocity profile for 300 kW

Figure 3: Isosurface of stoichiometric mixture fraction and predicted tangential velocity profile

Figure 4 shows the comparison between the predicted and measured maximum tangential velocity along the fire whirl height. The maximum tangential velocity, V_m, tends to be constant or increase slowly until $\frac{z}{D} = 1.25$, and then decreases with height, as observed in the experimental work of Lei *et al.* [30].

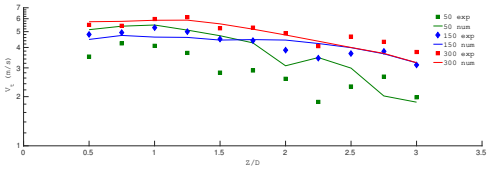

Figure 4: Numerical and experimental maximum tangential velocity versus height

Figure 5 shows the predicted and measured, Lei *el al.* [30], centreline excess temperature profile $(T - T_0)$. The numerical simulations are in agreement with the experiments up to the over fire plume zone. The same behaviour is present on the normalized centre line axial velocity (figure 6). The location where the velocity and temperature decrease

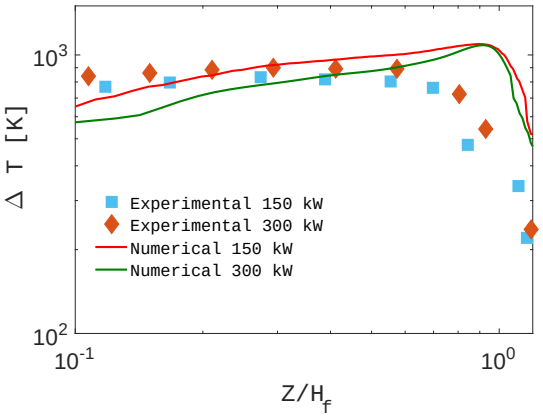

Figure 5: Centreline temperature profile

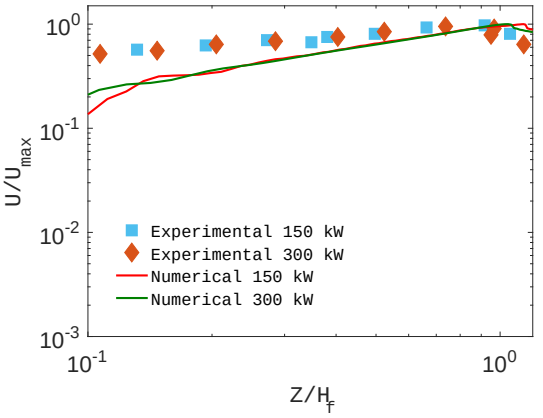

Figure 6: Centreline axial velocity profile

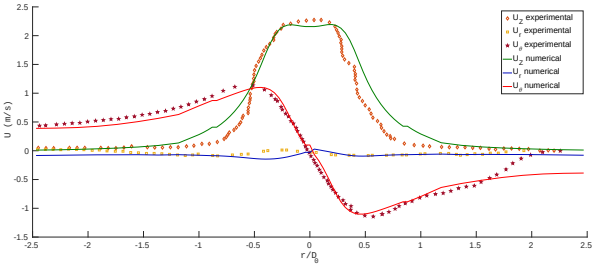

Figure 7: Axial, tangential and radial velocity profiles for $q = 2.19kW$.

correspond to the plume origin and the difference between prediction and measurements is attributed to temporal oscillations of the plume origin.

Small, $q = 2$ kW, fire whirls where also predicted and figure 7 shows the three velocity components along a radial line at $z/H = 0.2$. The obtained results agree well with the experimental observations from [4].

Table 2 lists the corresponding measured and predicted flame height for 2, 5, 50, 150 and 300 kW. The experimental continuous flame height is based on the location of the maximum centreline axial velocity. The criterion used in the numerical simulations are based on the stoichiometric mixture fraction that is consistent with experimental criterion. One should note that the measured flame height estimated from visual inspection of the flame is different from the value obtained by the location of time average centreline maximum axial velocity [30]. If the reference experiments are based on the average visual inspection, the error between the prediction and experiments are typically 15% in the range from 50 to 300 kW.

Power (kW)	Experimental (m)	Numerical (m)	Error (%)
2	0.347	0.362	4.32
5	0.591	0.578	2.20
50	1.31	1.33	1.53
150	3.19	3.31	3.76
300	4.33	4.45	2.77

Table 2: Flame height prediction and comparison with experimental data

4. Discussion

4.1. Flow Pattern

A typical fire whirl calculation for P=300 kW is presented at Figure 8 a) that shows isocontourns of the mean temperature and velocity vector in the flame vertical cross section. The maximum flame temperature is located at the shear layer near the flame origin while the centre of the fire whirl has a relatively lower temperature T=600 K, indicating a rich fuel zone. The gas burner inlet porous

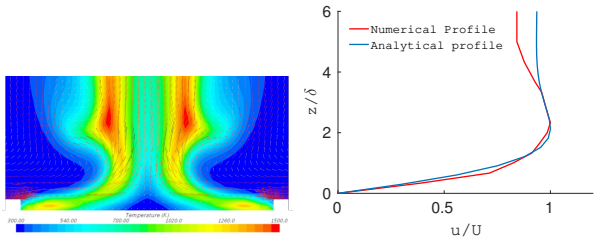

(a) Isocontours of temperature and velocity vectors

(b) Velocity profile

Figure 8: Predicted flame shape and flow patterns

configuration located below the fire whirl ground level allows for a natural influence of the air swirl

on the low momentum inlet fuel jet with Reynolds number equal to 2702. As a consequence, figure 8 a) shows a fuel jet behaviour similar to a pool fire with the narrowing conical shape of the fuel. This shape is consistent with an existence of an Ekman type inflow boundary layer [1, 3]. Figure 8 b) shows that the predicted velocity profile on the boundary layer over the ground floor is in agreement with an Ekman layer solution. The Ekman solution is an exact solution of the Navier-Stokes equations only valid for laminar flows. For turbulent flows there are two parameters in the analytical solution to be carefully evaluated, k_m and δ, being k_m the kinematic viscosity and $\delta = \sqrt{\frac{2K_m}{f}}$ the Ekman layer thickness, assuming a constant turbulent "eddy" viscosity, k_m and assuming the Coriolis parameter $f = \frac{2\pi}{T}$ with the period T obtained by the tangential velocity. The turbulent eddy viscosity was assumed to be given by $\nu_t = C_\mu \frac{\frac{1}{2}*(\overline{u'^2}+\overline{v'^2}+\overline{w'^2})}{\epsilon}$ with ϵ the turbulent dissipation rate and $C_\mu = 0.09$. The eddy viscosity is almost constant across the location of the Ekman layer and the prediction allow to estimate the modelled parameters as $k_m = 0.005m^2/s$, $f = 1.8s^{-1}$ and $\delta = 0.07m$. In spite of the gross assumption of the eddy diffusivity, δ was surprisingly in satisfactory agreement with the analytical Ekman solution as shown in figure 8 b).

4.2. Flame Height

The open literature and the previous results support the strong dependence of circulation on flame height. According to the Stokes theorem the circulation is the integral of the vorticity field, consequently, increasing the tangential momentum at the facility slits increases the vorticity field. To study the sensitivity of the fire whirl height to tangential air entrainment three burner heat releases (5, 150 and 300 kW) were considered. For each heat release the implicit mass flow entrainment was predicted and denoted as "naturally aspirated" mass flow rate. This is followed by increasing or decreasing the "naturally aspirated" air flow rate by prescribing a constant velocity boundary condition at the slits instead of a far hydrostatic pressure boundary condition.

The two approaches used to generate circulation, "prescribed mass flow" and "naturally aspirated", were considered for each non dimensional heat release Q^* obtained from dimensional analysis and derived from the Π non dimensional groups [3].

$$Q^* = \Pi_1 \times \Pi_6 = \frac{\dot{Q}}{\rho C_p \nabla T \sqrt{g L_h^3}} \qquad (12)$$

Analogously, for Γ^* the same procedure yields:

$$\Gamma^{=}\Pi_1 \times \frac{1}{\Pi_5} \times \Pi_{12} = \frac{U_z}{\sqrt{gL_h}} \times \frac{\Gamma}{U_r L_h} \times \frac{U_r}{U_z} = \frac{\Gamma}{L_h \sqrt{gL_h}} \qquad (13)$$

Figure 9 shows the prediction obtained for 5, 150

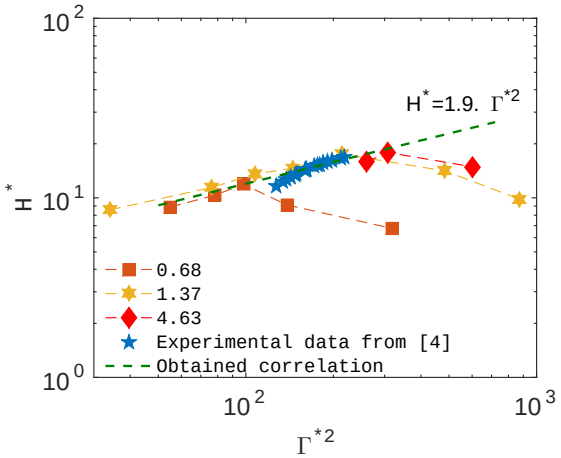

Figure 9: Correlation curve of fire whirl height H^* versus circulation Γ^*obtained from predictions and experimental data from [4]

and 300 kW using "naturally aspirated" entrainment and for each power several circulations were also obtained by prescribing mass flow at the slit inlet.

For each power it was predicted that the maximum flame height is reached for the "naturally aspirated" solution and the associated circulation denoted as critical circulation. The predicted trend is in agreement with the predictions of [16] and [18]

The predicted fire whirl height was correlated with the circulation considering only the "naturally aspirated" data and the data from [4]. The obtained correlation expressed by $H^* = 1.9\,(\Gamma^*)^{0.8}$ shares a similar slope with the one derived by Kuwana *et al.* [9], obtained from the numerical predictions of [16]. Figure 10 shows the isocontours of radial velocity on the fire whirl base. It is observed that the highest Γ^* value induces a greater radial velocity, suggesting an intensification of the promotion of the radial inflow with circulation. This is very important to the flow patterns that have to go around the flame expansion creating a wavy rotating stream around the fire whirl root.

Figure 11 shows the non-dimensional fuel mass flow $\dot{M}^* = \frac{\dot{m}}{\dot{m}_0}$ as a function of the flame height, obtained by integration of fuel concentration at several cross planes. The fuel consumption increases with circulation on the fire whirl base, suggesting an increase of air entrainment due the radial velocity component enhancement.

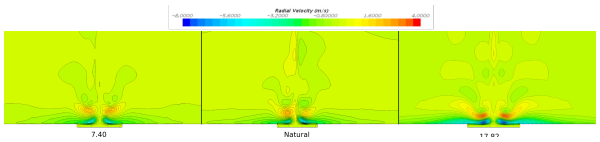

Figure 10: Isocountours of radial velocity on the fire whirl base for three circulation values

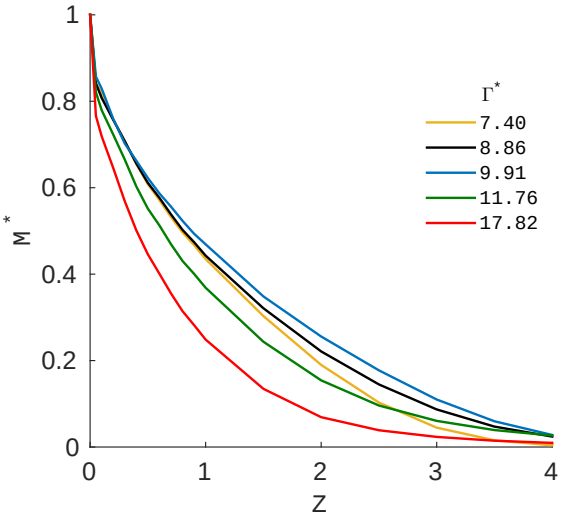

Figure 11: Non dimensional fuel mass flow vs height

4.3. Turbulence

Figure 12 a) shows the turbulent kinetic energy contour for a 300 kW non swirling diffusion flame and figure 12 b) shows the fire whirl case for 300 kW. The non swirling flame shows an increase of turbulent kinetic energy with height, reaching the highest values on the top of the flame. In contrast, the fire whirl presented larger values at the base, due to the gradients induced by the radial inflow layer. On the fire whirl body the values are much lower than in the analogous buoyant flame, suggesting the existence of turbulence suppression. Radial velocity fluctuations on the fire whirl are attenuated due to high centrifugal forces, decreasing turbulence compared with analogous non swirling flows.

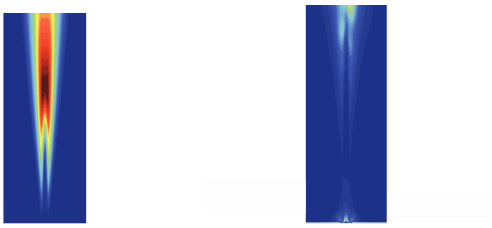

(a) Non swirling bouyant flame (b) Fire whirl

Figure 12: Predicted flame shape and flow patterns

The evolution of turbulence suppression has been analysed on light of Richardson number, due to the effect of swirl or streamline curvature on turbulent flow which is analogous to buoyancy [33, 34]. In this study we calculate the Richardson number (Ri) proposed by [35] based on the modelling of the ratio of mixing lengths with and without rotation. Figure 13 shows the predicted Richardson number along the centreline and the measured data from [35]. High values of Ri suggest turbulence suppression and the high Richardson values are predicted on the fire whirl bottom and they are consistent with experimental data from [35]. The turbulence generated at the fire whirl base is highly suppressed and with the increase in height the predicted Ri decrease with height according with the experimental observations, and the turbulent kinetic energy increases slightly, see figure 12 b) and 13.

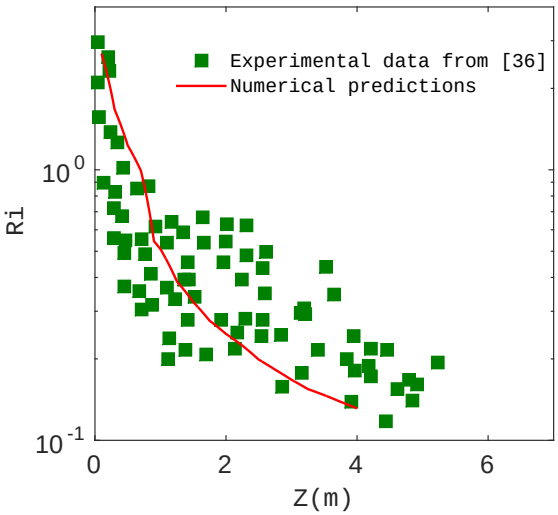

Figure 13: Richardson vs height from predictions and experimental data from [35]

5. Conclusions

Numerical simulations of laboratory fire whirls were conducted in order to validate and ascertain the effect of circulation on the flame structure. The Star-CCM+ code was employed with the turbulence Reynolds Stress Model. The boundary conditions used are physically bounded and together with the differential second order turbulence model allow to capture the averaged features from the base to the top of laboratory fire whirls. The simulations are in satisfactory agreement with experimental temperature and velocity along the radial and centreline profiles and with flame height.

It was shown that the Burgers vortex is a good description of the flow kinematics of fire whirls. The boundary layer present on the the floor is an Ekman type, which has a direct impact on the flow patterns

on the fire whirl base and fuel consumption.
The present study explored the effects of circulation on flame height. For each heat release considered a critical circulation was found that results in a maximum flame height. A correlation for the flame height dependence with circulation was deduced in good agreement with previous experiments and simulations.
The turbulence field of a fire whirl was compared with the analogous non swirling buoyant flame with the same fuel rate supply. The fire whirl presented smaller values of turbulent kinetic energy than the non swirling flame suggesting the effect of turbulence suppression.
The results show the potential for the use of RST approach to help achieve better understating of the fundamental knowledge of the driving mechanism and physical behaviour of fire whirls.

References

[1] Ritsu Dobashi, Tetsuya Okura, Ryosuke Nagaoka, Yasuhiro Hayashi, and Toshio Mogi. Experimental Study on Flame Height and Radiant Heat of Fire Whirls. *Fire Technology*, 52(4):1069–1080, 2016.

[2] Jason M. Forthofer and Scott L. Goodrick. Review of vortices in wildland fire, 2011.

[3] Ali Tohidi, Michael J. Gollner, and Huahua Xiao. Fire Whirls. *Annual Review of Fluid Mechanics*, 50(1):annurev–fluid–122316–045209, 2018.

[4] K. A. Hartl and A. J. Smits. Scaling of a small scale burner fire whirl. *Combustion and Flame*, 163:202–208, 2016.

[5] Jiao Lei, Congcong Ji, Naian Liu, and Linhe Zhang. Effect of imposed circulation on temperature and velocity in general fire whirl: An experimental investigation. *Proceedings of the Combustion Institute*, 000:1–8, 2018.

[6] Cláudia Pinto, Domingos Viegas, Miguel Almeida, and Jorge Raposo. Fire whirls in forest fires: An experimental analysis. *Fire Safety Journal*, 87(November 2016):37–48, 2017.

[7] Jiao Lei, Naian Liu, Linhe Zhang, Zhihua Deng, Nelson Kudzo Akafuah, Tianxiang Li, Kozo Saito, and Kohyu Satoh. Burning rates of liquid fuels in fire whirls. *Combustion and Flame*, 159(6):2104–2114, 2012.

[8] Jiao Lei, Naian Liu, and Kohyu Satoh. Buoyant pool fires under imposed circulations before the formation of fire whirls. *Proceedings of the Combustion Institute*, 2015.

[9] Kazunori Kuwana, Kozo Sekimoto, Kozo Saito, and Forman A. Williams. Scaling fire whirls. *Fire Safety Journal*, 43(4):252–257, 2008.

[10] S. Soma and K. Saito. Reconstruction of fire whirls using scale models. *Combustion and Flame*, 1991.

[11] Naian Liu, Qiong Liu, Zhihua Deng, Satoh Kohyu, and Jiping Zhu. Burn-out time data analysis on interaction effects among multiple fires in fire arrays. *Proceedings of the Combustion Institute*, 2007.

[12] P. B. Dermer, A. Y. Varaksin, and A. I. Leontiev. The wall-free non-stationary fire whirls generation by axisymmetric burning of solid fuel pellets. *International Journal of Heat and Mass Transfer*, 110:890–897, 2017.

[13] Rui Zhou and Zi Niu Wu. Fire whirls due to surrounding flame sources and the influence of the rotation speed on the flame height. *Journal of Fluid Mechanics*, 2007.

[14] Jiao Lei, Naian Liu, Linhe Zhang, Haixiang Chen, Lifu Shu, Pu Chen, Zhihua Deng, Jiping Zhu, Kohyu Satoh, and John L. De Ris. Experimental research on combustion dynamics of medium-scale fire whirl. *Proceedings of the Combustion Institute*, 2011.

[15] Hanyuan Yu, Song Guo, Minjun Peng, Quanwei Li, Jifeng Ruan, Wei Wan, and Chen Chen. Study on the influence of air-inlet width on fire whirls combustion characteristic. In *Procedia Engineering*, 2013.

[16] Francine Battaglia, Kevin B. McGrattan, Ronald G. Rehm, and Howard R. Baum. Simulating fire whirls. *Combustion Theory and Modelling*, 2000.

[17] A.Yu. Snegirev, J.A. Marsden, J. Francis, and G.M. Makhviladze. Numerical studies and experimental observations of whirling flames. *International Journal of Heat and Mass Transfer*, 47:2523–2539, 2004.

[18] Jiao Lei, Naian Liu, Yan Jiao, and Shaojie Zhang. Experimental investigation on flame patterns of buoyant diffusion flame in a large range of imposed circulations. *Proceedings of the Combustion Institute*, 36(2):3149–3156, 2017.

[19] Kuibin Zhou, Naian Liu, Jesse S. Lozano, Yanlong Shan, Bin Yao, and Kohyu Satoh. Effect of flow circulation on combustion dynamics of fire whirl. *Proceedings of the Combustion Institute*, 34(2):2617–2624, 2013.

[20] Howard W. Emmons and Shuh Jing Ying. The fire whirl. In *Symposium (International) on Combustion*, 1967.

[21] A. C.Y. Yuen, G. H. Yeoh, S. C.P. Cheung, Q. N. Chan, T. B.Y. Chen, W. Yang, and H. Lu. Numerical study of the development and angular speed of a small-scale fire whirl. *Journal of Computational Science*, 2018.

[22] W K Chow and S S Han. Experimental Data on Scale Modeling Studies on Internal Fire Whirls. 10(3):63–74, 2011.

[23] G. W. Zou and W. K. Chow. Generation of an internal fire whirl in an open roof vertical shaft model with a single corner gap. *Journal of Fire Sciences*, 2015.

[24] K. Hanjalić. One-Point Closure Models for Buoyancy-Driven Turbulent Flows. *Annual Review of Fluid Mechanics*, 2002.

[25] J. C F Pereira and J. M P Rocha. Simulation of shear orientation effects on stably stratified homogeneous turbulence with RANS second-order modelling. *Journal of Turbulence*, 10(43):1–35, 2009.

[26] J C F Pereira and J M P Rocha. Prediction of stably stratified homogeneous shear flows with second-order turbulence models. *Fluid Dynamics Research*, 42(4):45509, 2010.

[27] D. B. Spalding. Mixing and chemical reaction in steady confined turbulent flames. *Symposium (International) on Combustion*, 1971.

[28] B. F. Magnussen and B. H. Hjertager. On mathematical modeling of turbulent combustion with special emphasis on soot formation and combustion. *Symposium (International) on Combustion*, 1977.

[29] J. M.C. Pereira, J. E.P. Navalho, A. C.G. Amador, and J. C.F. Pereira. Multi-scale modeling of diffusion and reaction-diffusion phenomena in catalytic porous layers: Comparison with the 1D approach. *Chemical Engineering Science*, 2014.

[30] Jiao Lei, Naian Liu, Linhe Zhang, and Kohyu Satoh. Temperature, velocity and air entrainment of fire whirl plume: A comprehensive experimental investigation. *Combustion and Flame*, 162(3):745–758, 2015.

[31] A. Y. Klimenko and F. A. Williams. On the flame length in firewhirls with strong vorticity. *Combustion and Flame*, 2013.

[32] W. K. Chow, Z. He, and Y. Gao. Internal fire whirls in a vertical shaft. *Journal of Fire Sciences*, 2011.

[33] David G. Lilley. Prediction of Inert Turbulent Swirl Flows. *AIAA Journal*, 11(7):955–960, 1973.

[34] J. M. Beér, N. A. Chigier, T. W. Davies, and K. Bassindale. Laminarization of turbulent flames in rotating environments. *Combustion and Flame*, 1971.

[35] Jiao Lei, Naian Liu, and Ran Tu. Flame height of turbulent fire whirls: A model study by concept of turbulence suppression. *Proceedings of the Combustion Institute*, 2017.